Real-time forecasting of solar wind high-speed streams

Astrid M. Veronig[1, ✉], T. Rotter[1], M. Temmer[1], M. Reiss[1], S. Hofmeister[1] and B. Vršnak[2] ; ✉ astrid.veronig@uni-graz.at

[1] Institute of Physics/Kanzelhöhe Observatory, University of Graz, Austria
[2] Hvar Observatory, University of Zagreb, Croatia

Introduction

The Sun's corona is constantly emanating magnetized plasma into space, the solar wind consisting of charged particles (protons, electrons, Helium ions). The slow solar wind has typical speeds in the range 300–400 km s^{-1}, whereas the so-called high-speed solar wind streams (HSSs) originating from coronal holes may reach speeds up to 800 km s^{-1} (e.g., Krieger et al. 1973). Studying coronal holes (CHs) and their associated HSSs is an important task, since a) in combination with the Sun's rotation they shape the solar wind distribution in interplanetary space, b) at times of low solar activity they are the dominant contributors to space weather disturbances due to recurrent geomagnetic storm activity, c) they affect the interplanetary propagation and arrival time predictions of coronal mass ejections. In this poster, we present an empirical method that relates the coronal hole area on the Sun to the solar wind speed at 1 AU. This method is in use to predict the background solar wind speed at 1 AU with a lead time of about 4 days from quasi real-time SDO/AIA extreme-ultraviolet images, `http://swe.uni-graz.at/solarwind/`.

Data and Methods

We use SDO/AIA 193 Å (Lemen et al. 2012) 1k×1k quicklook images with a 1-hour cadence to extract the fractional coronal hole area A over a 15° slice centered at the central meridian. The method applies histogram-based thresholding techniques followed by erosion and dilation operators (Rotter et al. 2012), see Figure 1.

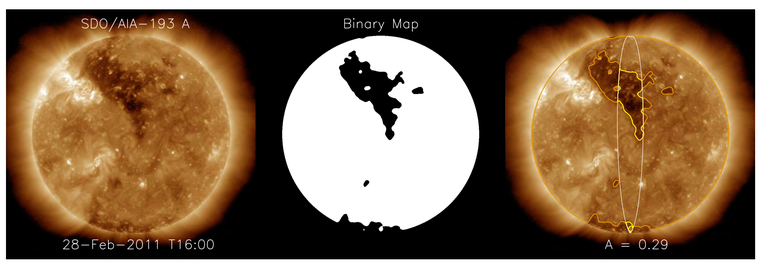

Figure 1: **Left:** Sample SDO/AIA 193 Å image. **Middle:** Binary map resulting from the CH segmentation algorithm. **Right:** CH binary map overlayed on AIA image. The yellow lines mark the derived CH area within the 15° meridional slice.

The forecast (Fig. 2b) is based on deriving the delay between the fractional CH area time series $A(t)$ (Fig. 2a) and the solar wind speed $v(t)$ measured by ACE using cross-correlation (Fig. 2c). To predict the solar wind speed, we shift the CH area time series with the derived lag τ and apply a linear function $v(t+\tau) = c_0 + c_1 A(t)$ (cf. Vršnak et al. 2007). The parameters c_0 and c_1 are obtained by searching for the minimum and maximum values of the solar wind speeds and the corresponding CH fractional areas in preceding periods (Fig. 2d). Speeds >800 km s^{-1} are excluded, as they most probably arise due to interplanetary CMEs and not due to HSS. To account for variations over the solar cycle, the algorithm is automatically adapted by using the information from the 3 preceding Carrington Rotations (CRs) to update the prediction parameters c_0 and c_1.

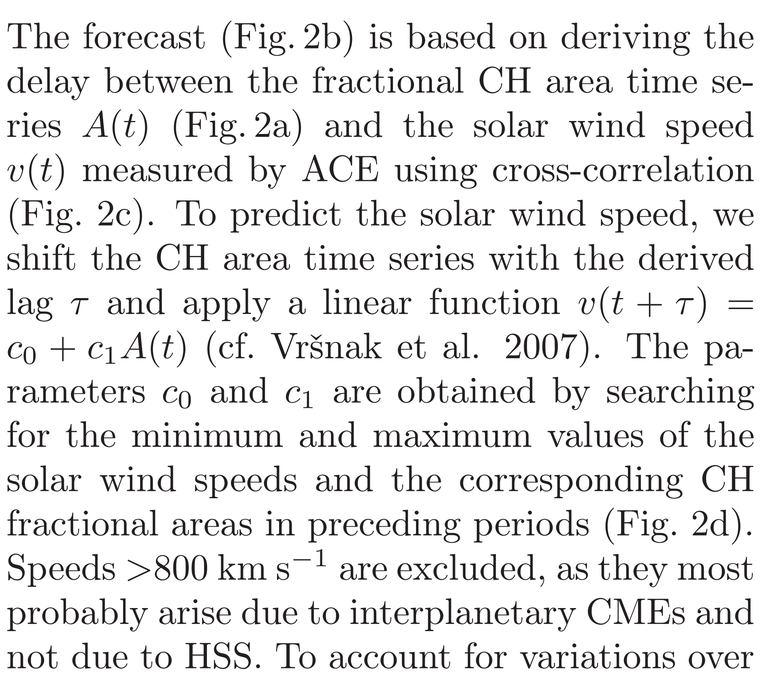

Figure 2: Illustration of the algorithm to predict solar wind speed v from measured CH areas A.

Results

Figure 3 shows the solar wind speed predictions based on the adaptive algorithm together with in situ measurements by ACE at 1 AU for the years 2011 to 2013. ICMEs that passed over the ACE spacecraft are also indicated, based on the ICME list compiled by Richardson and Cane (`http://www.srl.caltech.edu/ACE/ASC/DATA/level3/icmetable2.htm`). The mean of the time lags between CH fractional area time series and solar wind speeds applied in the predictions is 4.0 ± 0.5 days.

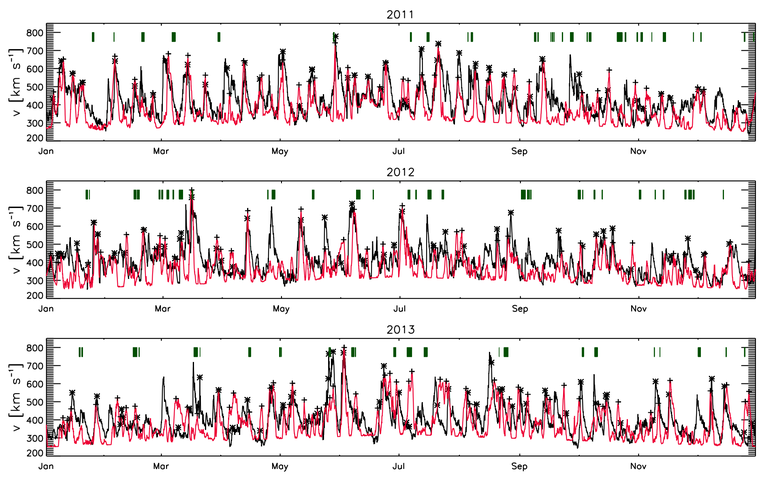

Figure 3: Solar wind speed measured by ACE (black lines) and predicted from the CH areas (red lines). Cross-signs (stars) indicate peaks in the predicted (measured) solar wind speed. Green bars highlight ICME occurrence.

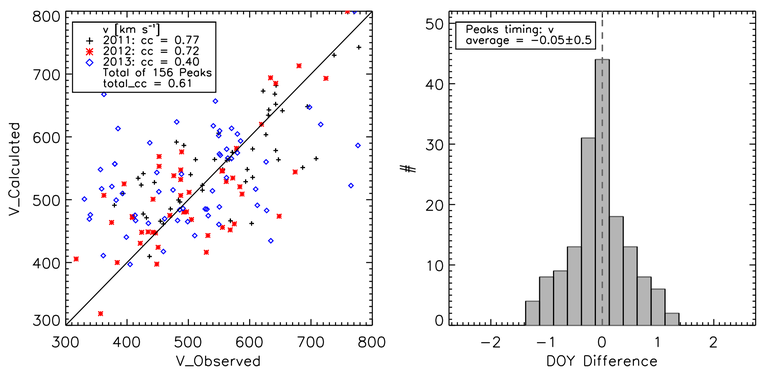

Figure 4: **Left:** Scatter plot of predicted versus measured peaks in the solar wind speed. The one-to-one correspondence is plotted as a black line. **Right:** Histograms of the difference between measured and predicted peak arrival times.

In Figure 4 (left panel) we show the predicted versus measured solar wind speed at 1 AU derived from 156 peaks identified. The overall correlation coefficient gives $cc = 0.61$. The correlation coefficients for the individual years are 0.77 (2011), 0.72 (2012) and 0.40 (2013). The right panel shows the distribution of the differences of the arrival times of the peaks in the solar wind speed measurements and predictions. The distribution peaks at zero, with a mean difference of -0.05 ± 0.50 days. In 80% of the 156 peaks identified, the predicted arrival times lie within ±0.5 days of the measurements.

Discussion and Conclusions

The adaptive algorithm delivers reliable predictions for peaks in the undisturbed solar wind speed (i.e. not affected by ICMEs) with a lead time of 4 days. The prediction accuracy of the HSS arrival times lies within ±0.5 days in 80% of the cases. The predicted amplitudes reveal a correlation of $cc = 0.6$ over the three years under study. Predictions for the solar wind speed peaks at 1 AU based on this empirical model are thus comparable to numerical models such as ENLIL and WSA (tested for the year 2007 by Gressl et al. 2014).

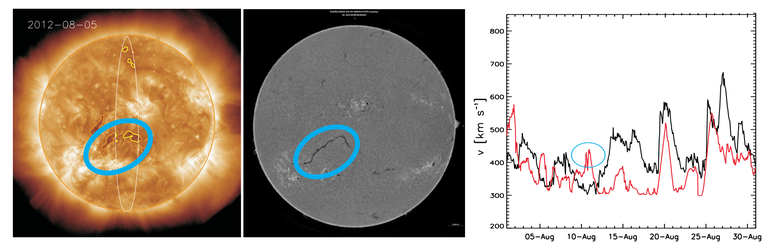

Figure 5: **Left**: SDO/AIA 193 Å image from 5th August 2012 together with the coronal hole areas detected. **Middle:** Hα image from Kanzelhöhe Observatory. **Right:** ACE solar wind measurements (black line) and predictions (red line). The blue ellipse highlights the filament that is erroneously detected as CH in the AIA image, thus causing an erroneous peak in the solar wind predictions.

Figure 5 illustrates that unreliable solar wind predictions can be caused by erroneous CH detection. The comparison with Hα filtergrams shows that sometimes filament channels are identified by the CH segmentation, as they are both characterized by low intensities in the EUV images. We are currently developing classification models based on the geometry and magnetic field characteristics to better distinguish filaments from CHs in EUV images (Reiss et al. 2014; poster no. 2). A detailed description of the adaptive solar wind forecast method presented here can be found in Rotter et al. (2014) and is tested on real-time data, available at `http://swe.uni-graz.at/solarwind/`.

References

- Krieger et al. 1973, Solar Phys. 29, 505
- Gressl et al. 2014, Solar Phys. 289, 1883
- Lemen et al. 2012, Solar Phys. 275, 17
- Reiss et al. 2014, CEAB, in press
- Rotter et al. 2012, Solar Phys. 281, 793
- Rotter et al. 2014, Solar Phys., submitted
- Vršnak et al. 2007, Solar Phys. 240, 315

Acknowledgments

This study has received funding from the European Commission's Seventh Framework Programme (FP7/2007-2013) under the grant agreement no. 284461 [eHEROES] and no. 263252 [COMESEP].